catalysts

MDPI

Article

Core-Shell Structured Ni@SiO_2 Catalysts Exhibiting Excellent Catalytic Performance for Syngas Methanation Reactions

Yang Han [1], Bo Wen [1] and Mingyuan Zhu [1,2,*]

[1] School of Chemistry and Chemical Engineering of Shihezi University, Shihezi 832000, Xinjiang, China; llccnn@stu.shzu.edu.cn (Y.H.); owenbo@stu.shzu.edu.cn (B.W.)

[2] Key Laboratory for Green Processing of Chemical Engineering of Xinjiang Bingtuan, Shihezi 832000, Xinjiang, China

* Correspondence: zhuminyuan@shzu.edu.cn; Tel.: +86-993-2057277

Academic Editors: Benoît Louis, Qiang Wang and Marcelo Maciel Pereira

Received: 24 November 2016; Accepted: 5 January 2017; Published: 9 January 2017

Abstract: In this study, we prepared core-shell structured Ni@SiO_2 catalysts using chemical precipitation and modified Stöber methods. The obtained Ni@SiO_2 samples exhibited excellent catalysis performances, including high CO conversion of 99.0% and CH_4 yield of 89.8%. Moreover, Ni@SiO_2 exhibited excellent catalytic stability during a 100 h lifetime test, which was superior to that of the Ni/SiO_2 catalyst. The prepared samples were characterized using a series of techniques, and the results indicated that the catalytic performance for syngas methanation reaction of the Ni@SiO_2 sample was markedly improved owing to its nanoreactor structure. The strong interaction between the Ni core and the SiO_2 shell effectively restrained the growth of particles, and the deposition of C species.

Keywords: syngas methanation; Ni@SiO_2; anti-carbon deposition; catalytic stability

1. Introduction

Today's society faces many energy challenges, including environmental pollution, expensive crude oil prices, and short supply of natural gas resources [1]. Natural gas is a promising energy source as it is good quality fuel and a chemical raw material. Over the past decade, the coal gasification method for preparing synthetic gas has been extensively investigated. CO methanation is one of the most important reactions investigated for this process [2–6].

Conversion of coal to methane via gasification and methanation processes can not only utilize the abundant coal resources but also meet the rapidly growing demand for natural gas in coal-rich regions or countries [7]. The methanation of syngas has been considered as the most critical step in the processing of coal to produce synthetic natural gas [8–10]. In recent years, highly efficient and stable catalysts for syngas methanation have been developed.

Noble metals, such as Pd, Rh, and Ru, exhibit high chemical stability and excellent activity for syngas methanation at low temperatures [11–13]. However, the limited reserves and high prices of noble metals greatly limit their industrial applications. Owing to the excellent activity as comparable to the noble metal catalysts and the low-cost, Ni-based catalysts have been widely used for syngas methantion [14]. However, using conventional Ni-based catalysts still has enormous challenges. The methanation of CO is a highly exothermic process; hence, the heat produced on the surface of the catalyst would cause serious problems, such as C deposition and aggregation of Ni nanoparticles.

In recent years, catalysts with a core-shell structure have been widely used in various catalysis fields. The metal component of active nanoparticles is coated with an inert nanoporous oxide shell, and the outer shells effectively protect the active nanoparticle cores from sintering when reactions

are performed at high temperature. The unique physical and/or chemical interactions can result in synergic effects. Chao Wang et al. [15] successfully synthesized the Ni@graphene composites comprising a graphene shell and a Ni metal core using an arc-discharge method. The outer carbon sheath prevents the inner Ni nanoparticle from being etched when the sample is exposed to air, H_2O_2, or acids. Takenaka et al. [16] reported that a SiO_2-coated nickel-based catalyst exhibited excellent catalytic performance and good stability in partial oxidation of methane (POM) reaction, as compared with conventional Ni/Al_2O_3. Li et al. [17] synthesized Ni@meso-SiO_2 catalysts exhibiting excellent catalytic performance in the POM reaction to synthesize gas. Ni particles encapsulated in core–shell structured catalysts exhibited high catalytic activities and enhanced inhibition toward C deposition [18,19]. Li et al. [20] successfully synthesized transition metal (Ni, Cu, Co) coated in hollow zeolite single crystals by recrystallization and impregnated method, in hydrogenation reaction, coated Ni particles showed excellent size-selectivity performance. Based on the above-mentioned studies, it can be inferred that $Ni@SiO_2$ with active Ni as the core and SiO_2 as the coated shell may exhibit excellent catalytic performance in CO methanation, owing to its unique structure.

Herein, we report the synthesis of $Ni@SiO_2$ catalysts as well as their catalytic activity and stability for methanation reaction at different temperatures. Characterization methods, such as N_2 physical adsorption, X-ray diffraction (XRD), hydrogen temperature-programmed reduction (H_2-TPR), thermo-gravimetric analysis (TGA), and transmission electron microscopy (TEM), were employed for understanding the relationship between the catalytic performance and the physical structure of the catalyst.

2. Results and Discussion

2.1. Characterization of the Catalysts

Figure 1 shows the XRD results obtained for $NiO@SiO_2$ and NiO/SiO_2, revealing that both the catalysts exhibited similar diffraction peaks. The diffraction peaks observed at 2θ = 37.3°, 43.2°, and 63.9° could be attributed to (111), (200), and (220) of the NiO phase, respectively (JCPDS No. 78-0429). There could still be oxidized nickel species present as amorphous phases or clusters too small to be observed by XRD. Figure 2 shows the XRD pattern of the catalyst obtained after performing in situ reduction. The peaks observed at 44.3°, 52.5°, and 76.8°correspond to the typical crystalline planes of Ni, indicating that NiO was completely reduced to Ni metal. XRD results show that the NiO and Ni nanoparticles in the core-shell catalyst before and after reduction exhibit a smaller grain size.

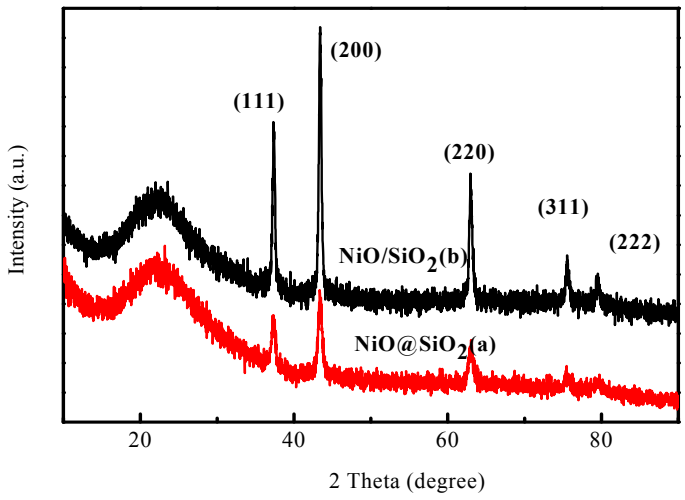

Figure 1. XRD (X-ray diffraction) patterns of the as-obtained $NiO@SiO_2$ (**a**); and NiO/SiO_2 (**b**) catalysts.

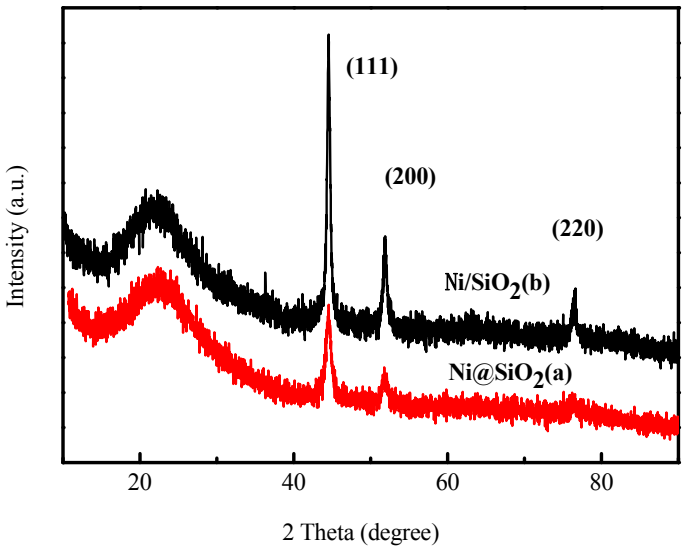

Figure 2. XRD patterns of the Ni@SiO_2 (**a**); and Ni/SiO_2 (**b**) catalysts both after situ reduction.

The surface area, pore volume, and average pore size of NiO@SiO_2 and NiO/SiO_2 are shown in Table 1. The core-shell structured NiO@SiO_2 exhibits a larger surface area and pore size. This could be because the NiO particles filled and blocked some of the silica pores in the NiO/SiO_2 samples. The core-shell structured NiO@SiO_2 catalysts exhibited smaller NiO crystallite sizes, as well as a modified SiO_2 texture. The porous SiO_2 shell allows the free access and transfer of gaseous reactant and product molecules. Thus, core-shell structures comprising metal particles on high surface area supports are known to be the most effective heterogeneous catalysts [21].

Table 1. Characteristics of NiO@SiO_2 and NiO/SiO_2 samples determined by N_2 sorption and XRD.

Samples	BET Surface Area (m^2/g) [a]	Pore Volume (cm^3/g) [b]	Average Pore Size (nm) [c]	Metal Crystallite (nm) [d]
NiO@SiO_2	263	0.79	12.1	8.6
NiO/SiO_2	162	0.14	3.5	19.8

[a] Calculated by the Brunauer–Emmett–Teller (BET) equation; [b] Barrett-Joyner-Halenda(BJH) desorption pore volume; [c] BJH desorption average pore size; [d] Calculated from Ni(111) plane by Scherrer's equation.

Figure 3a,b illustrates the Transmission Electron Microscopy (TEM) image and the morphological features of the NiO@SiO_2 and NiO/SiO_2 samples. By examining 50–100 NiO particles, the diameter of the NiO cores in NiO@SiO_2 catalyst is calculated to be ~11.2 nm, which is much smaller than that of NiO/SiO_2 (28.7 nm). HAADF-STEM measurements confirmed the existence of the core-shell structure. From Figure 3c,d, the distribution of the catalyst supports and the active components in the two samples seems to be significantly different. In case of the NiO@SiO_2 catalyst, NiO core is evenly distributed on the SiO_2 shell, whereas NiO nano-particles are distributed on the silica spheres in the case of the NiO/SiO_2 sample. Figure 3e,f shows the TEM images of NiO@SiO_2 and NiO/SiO_2 both after hydrogen treatment, the core-shell structure of NiO@SiO_2 sample can be well maintained after treated at 550 °C, 20% H_2/Ar for 3 h, and the NiO nanoparticles are uniformly dispersed without obvious agglomeration. For NiO/SiO_2, the aggregation of NiO nanoparticles appeared.

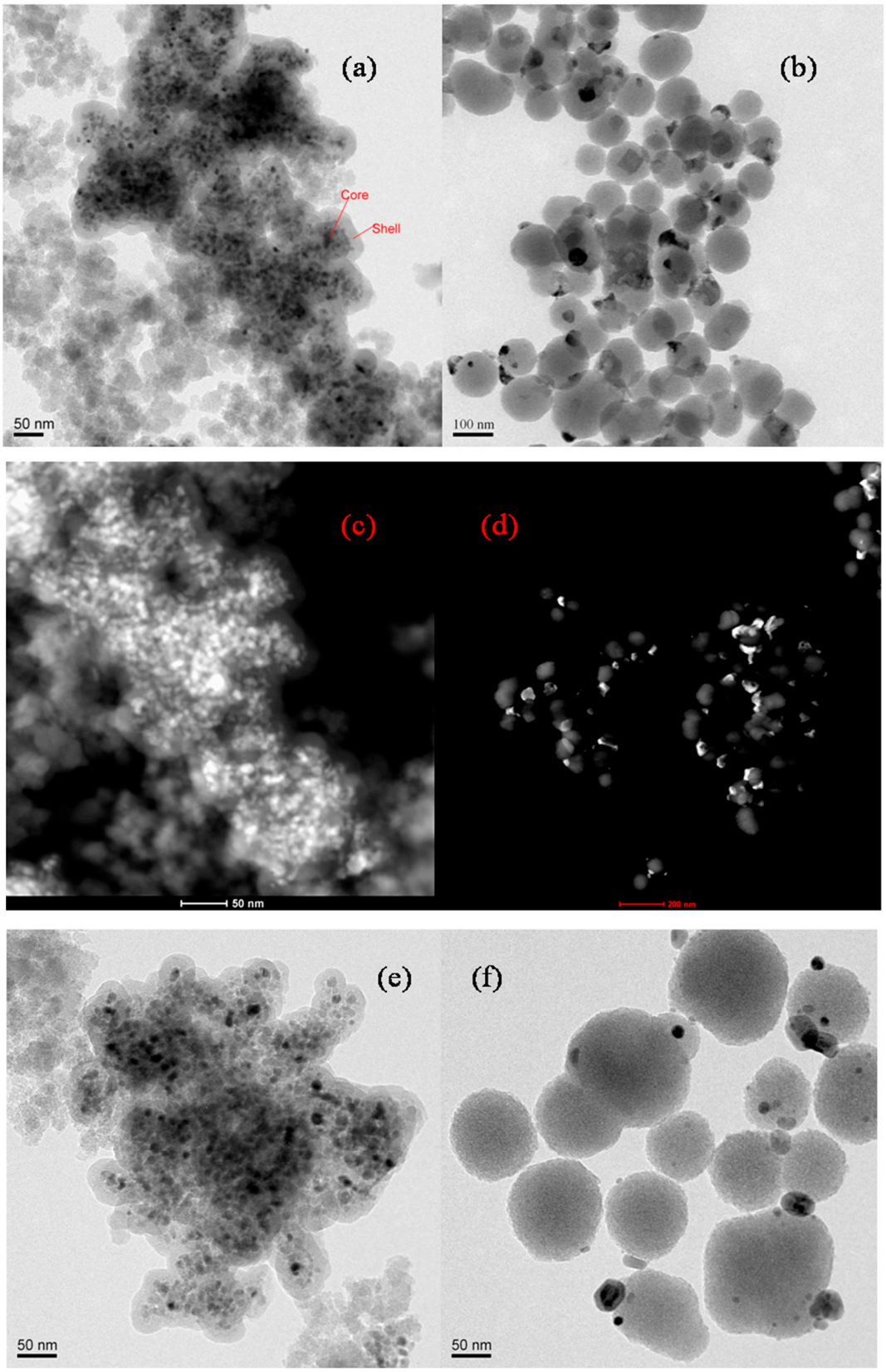

Figure 3. Transmission Electron Microscopy (TEM) images of as-obtained (**a**) NiO@SiO_2; (**b**) NiO/SiO_2; HAADF-STEM image of (**c**) NiO@SiO_2 and (**d**) NiO/SiO_2; TEM images of samples (**e**) NiO@SiO_2 and (**f**) NiO/SiO_2, both after hydrogen treatment at 550 °C, 3 h.

H_2 Temperature Programmed Reduction (H_2-TPR) technique was employed in order to study the reduction behavior of supported oxide catalysts, and determine the effect of the core-shell structure on NiO encapsulation in the SiO_2 support, as well as the catalytic performance of the samples. In the case of NiO/SiO_2, the NiO reduction peak is observed at a lower temperature (200–400 °C), while the H_2 reduction peak obtained for the NiO@SiO_2 catalyst can be divided into two peaks (Figure 4) the first peak observed in the range of 200–320 °C is associated with the NiO species and pure NiO [4]. In this case, the interaction between NiO and SiO_2 is relatively weak [22], the second peak observed in the temperature range of 350–600 °C is associated with the NiO species forcefully interacted with the SiO_2 support [16]. These results demonstrate that the interaction between the NiO nano-particles and the SiO_2 support becomes stronger after the encapsulation, which consistently matches the pioneer's results [19,23]. The formation of this NiO species, which strongly interacted with coated SiO_2, would enhance the catalytic performance and life for the syngas methanation reaction.

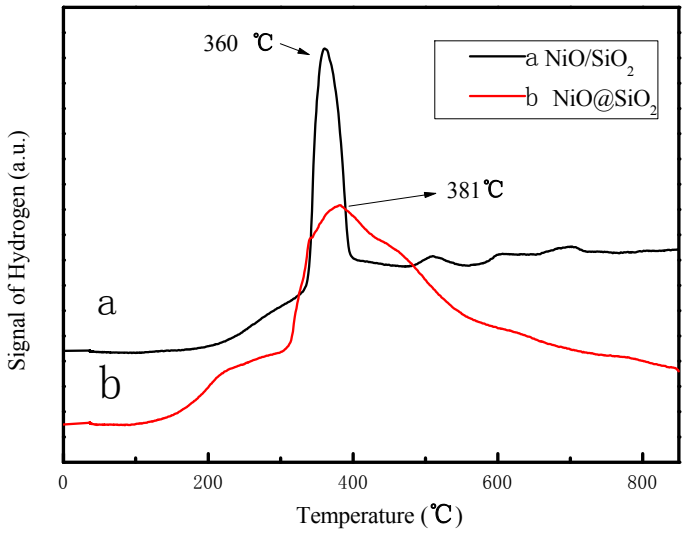

Figure 4. H_2 Temperature Programmed Reduction (H_2-TPR) profiles of (**a**) NiO@SiO_2 and (**b**) NiO/SiO_2.

2.2. Catalytic Performances of the Catalysts

The catalytic performance of the samples was tested under 1.5 MPa in the test temperature range of 250–550 °C. Figure 5A shows the results obtained for the Ni@SiO_2 catalyst in the temperature range of 250–500 °C, demonstrating the maximum CO conversion, close to 100%. In the case of the Ni/SiO_2 catalyst, the best activity was achieved in a narrow temperature range of 400–450 °C which is slightly lower than that of the Ni@SiO_2 catalyst. Due to the influence of kinetic factors, the CO conversion increased with an increase in the temperature at the low temperature range. However, due to the limitation of thermodynamic equilibrium, the CO conversion decreased at the high-temperature range [24]. Figure 5B illustrates the CH_4 yield comparison of different samples. For both of the catalysts, the yield of CH_4 increased with an increase in the reaction temperature before reducing the samples, which could be attributed to the thermodynamic limitation. As the two samples prepared using different methods exhibited different structures, we speculate that the catalytic performance could be greatly influenced by the structure of the catalyst. When the same amount of Ni was used (10 wt %), the catalyst with the core-shell structure exhibited a higher CO conversion and CH_4 yield.

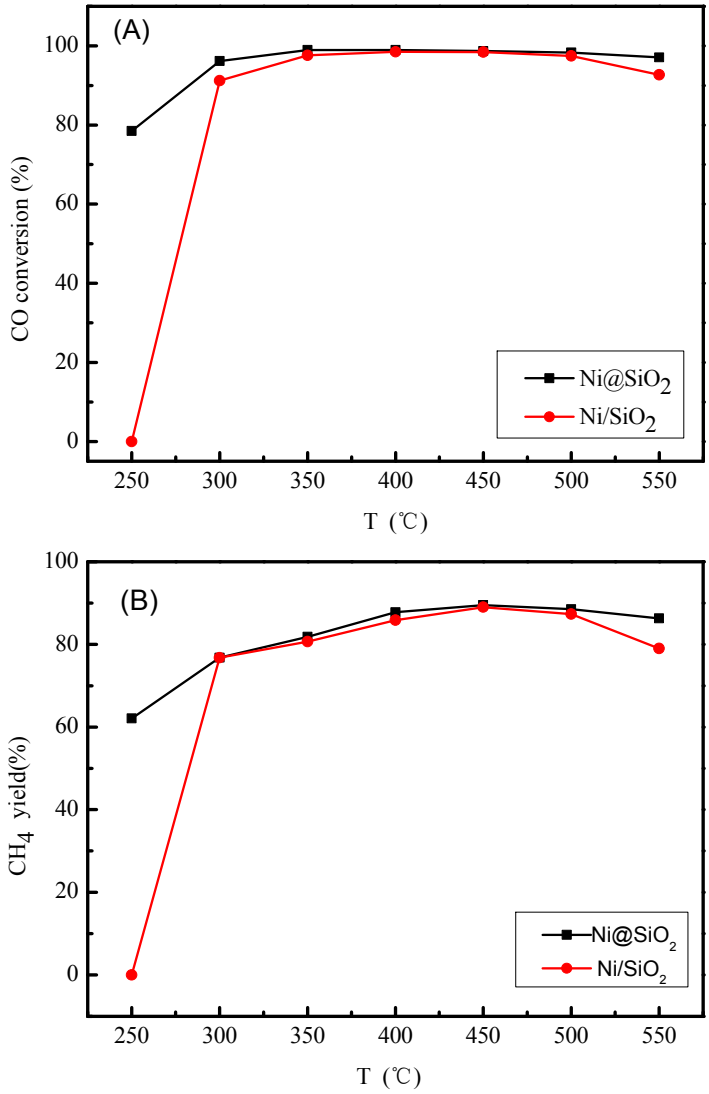

Figure 5. CO conversion (**A**) and CH_4 yield (**B**) of the $Ni@SiO_2$ and Ni/SiO_2 catalysts at 1.5 MPa, 36,000 mL/g/h.

On examining the results obtained with the catalyst performance test and the XRD, TEM, and TPR measurements, samples containing small NiO particles are found to exhibit an excellent catalyst performance. The sintering of the Ni core can be effectively reduced owing to the narrow space between the core and the shell as a strong interaction might cause an increase in the reduction temperature of catalyst, TPR analysis results support our speculation [23]. Amphipathic and non-ionic PVP polymers can be adsorbed on colloidal particles, and PVP have been commonly employed in the preparation of mesoporous samples. On the other hand, the good dispersity of the active component could be helpful in the formation of uniform pores. The uniform pores are also conducive to the entering of reactant and product [17,23].

2.3. Stability of the Catalysts

The 100 h lifetime test was conducted at 500 °C under a pressure of 1.5 MPa, and Gas Hour Space Velocity (GHSV) = 36,000 h^{-1} and the test results are displayed in Figure 6 For $Ni@SiO_2$, no obvious decrease in the CO conversion is observed with the in 100 h stability test. For the Ni/SiO_2 catalyst, the CO conversion is significantly decreased after 12 h. Thus, $Ni@SiO_2$ exhibited excellent stability under selected reaction conditions.

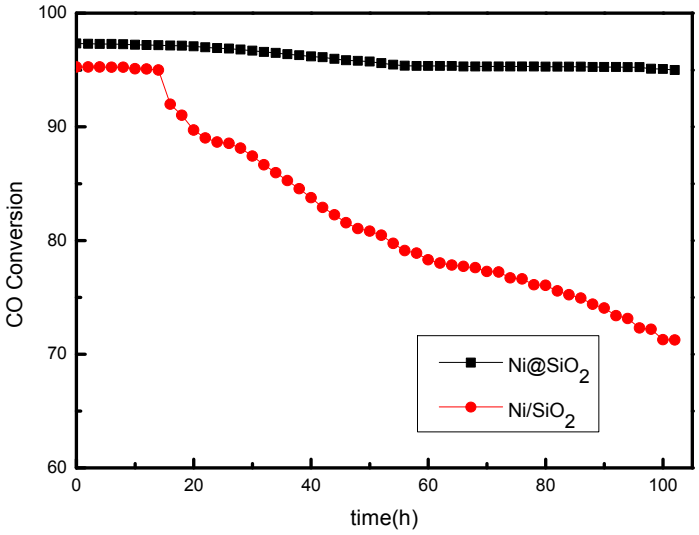

Figure 6. Stability of the Ni@SiO_2 catalyst for CO methanation at 500 °C, 1.5 MPa, 36,000 mL/g/h.

2.4. Characterization of the Used Catalysts

Figure 7a,b demonstrate the TEM image of NiO@SiO_2 and Ni/SiO_2catalysts obtained after performing the activity test. The average particle size of the NiO encapsulated in SiO_2 sample is around 27.1 nm, and the diameter of NiO on the surface of the silica particles is around 45.3 nm. Since it is difficult to achieve complete individual particle encapsulation, there is a degree of aggregation in the NiO@SiO_2 catalyst after the reaction, this result is consistent with the literature [16,23]. The NiO@SiO_2 catalyst exhibits a smaller particle size and a higher uniform dispersion than those of NiO/SiO_2, indicating that the SiO_2 shell effectively protects the NiO cores, in the calcination process performed at high temperatures. Exposed metal nanoparticles are commonly air-sensitive [16]; however, after coating metal nanoparticles with SiO_2, their thermal stability improves [25]. From the TPR results, owing to the stronger interaction between the NiO core and the SiO_2 shell, the inhibition of the active component of Ni aggregationin the reaction process.

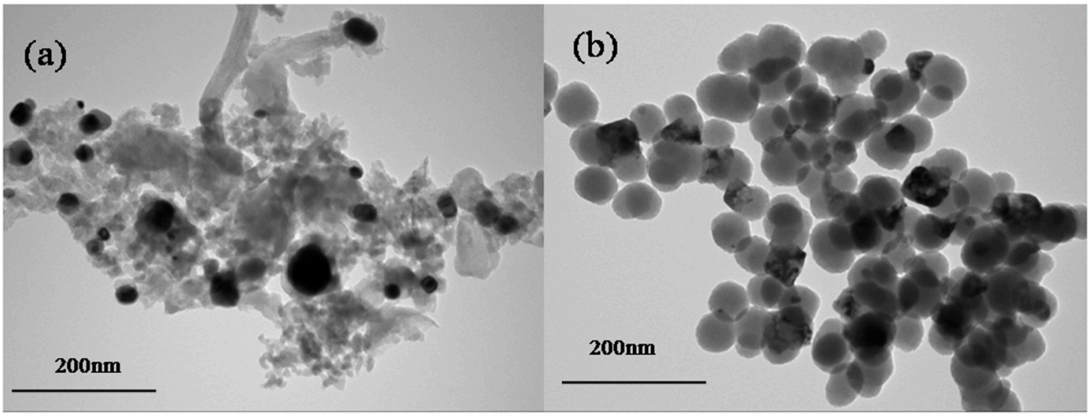

Figure 7. TEM images of used catalysts (**a**) NiO@SiO_2; and (**b**) NiO/SiO_2.

The TGA curves of the Ni-based catalysts obtained after performing the lifetime test are shown in Figure 8. TGA curves indicate the weight loss of the samples at two temperature ranges. The first weight loss was observed below 400 °C due to the removal of organic components and physically adsorbed water molecules. The second weight loss observed could be associated to the oxidation of graphitized C species occurred in the 400–600 °C range [26,27]. In the TGA test temperature range,

the weight of the Ni@SiO_2 catalyst sample reduces approximately by 8.94%, which could be attributed to the production of C that probably causes reduction in catalyst activity as obtained in the performance test. However, the weight of the Ni/SiO_2 catalyst sample is reduced by 56.73%, demonstrating that the C deposition occurs easily at the Ni/SiO_2 catalyst surface by encapsulating Ni nanoparticles in the SiO_2 support, the C deposition behavior is clearly changed. The strong interactionbetween the Ni core and the SiO_2 shell effectively inhibits the formation of C deposits. TGA analysis provides evidence for the excellent CO conversion for Ni@SiO_2 obtained in the 100-h lifetime activity test.

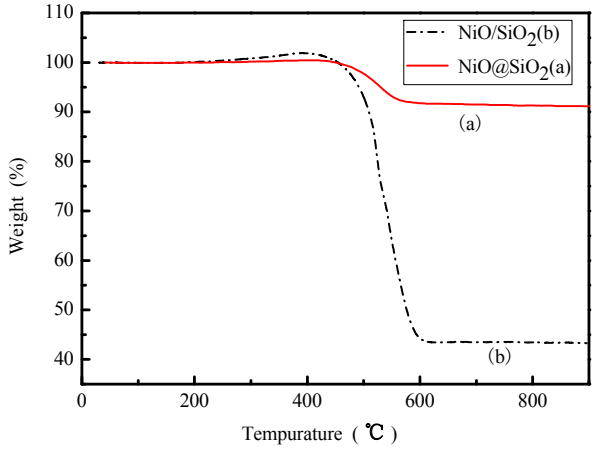

Figure 8. thermo-gravimetric analysis (TGA) profiles of used catalysts after 100 h lifetime test for (a) NiO@SiO_2 and (b) NiO/SiO_2.

3. Experimental

3.1. Catalyst Preparation

Nickel nitrate (Ni $(NO_3)_2 \cdot 6H_2O$) was acquired from Aladdin (Aladdin Industrial Corporation, Los Angeles, Southern CA, USA), and polyethylene glycol (PEG) (average MW = 20,000) and $NH_3 \cdot H_2O$ (25 wt %) were obtained from Chengdu Kelong Chemical Reagent Factory. Tetraethylorthosilicate (TEOS, SiO_2, 28%) was purchased from Tianjin Da mao Chemical Reagent Factory, Tianjin, China. Sodium hydroxide (NaOH) was obtained from Tianjin Yong Sheng Fine Chemical Co., Ltd., Tianjin, China. Absolute ethyl alcohol was acquired from Tianjin Fu Yu Fine Chemical Co., Ltd., Tianjin, China. All of the materials used in this study were of AR grade and were directly used without any further purification.

3.1.1. Preparation of Ni@SiO_2 Catalyst

The catalyst was prepared in two steps. In the first step, NiO nanoparticles were prepared using a chemical precipitation method. The preparation procedure can be described as follows: 330 mg PEG (average MW = 20,000) and 1.0 g NaOH was dissolved in 100 mL deionized water. Subsequently, 2.9 g nickel nitrate was added to 40 mL deionized water, and the obtained solution was added dropwise to the NaOH solution. The obtained mixture was stirred for 2 h. The solid product obtained was collected by suction filtration and washed with absolute ethyl alcohol and deionized water several times. The product was dried at 50 °C for 24 h followed by subjecting to calcinations at 450 °C for 2 h.

In the second step, NiO@SiO_2 was prepared using a modified Stöber method [28,29]. In a typical reaction, 0.2 g of the prepared NiO nanoparticles, 1.0 g PVP (K30), and 100 mL anhydrous ethanol were mixed and stirred for 12 h. 10 mL of aqueous solution of ammonia (28%) was added to this solution, followed by sonicating the suspension for 0.5 h. Subsequently, TEOS (SiO_2, 28%) was dissolved in 5 mL anhydrous ethanol in desired amounts at room temperature. This solution was then injected into the suspension. After 1 h, the product was isolated by centrifugation and washed with ethanol, followed

by drying in air at 80 °C for 6 h. The sample was than calcined at 550 °C for 3 h in air. The coated sample thus obtained is named as NiO@SiO_2.

3.1.2. Preparation of Ni/SiO_2 Catalyst

For comparison purposes, SiO_2 support was prepared by the modified Stöber method. The same procedure as the second step was used. The Ni/SiO_2 was prepared using a conventional impregnation method as reported earlier [30]. The loading of nickel in Ni@SiO_2 and Ni/SiO_2 catalysts is the same, both are 10 wt %.

3.2. Catalyst Characterization

Powder XRD measurements were carried out in order to examine the crystal structure of the Ni-based catalyst. With a Bruker Advanced D8 X-ray diffractometer using Cu-Kα irradiation (λ = 1.5406 Å) as the X-ray source at 40 kV and 40 mA. An angular range of 10°–90° was employed with a step size of 0.02. The grain size was calculated using Scherrer's formula.

Brunauer–Emmett–Teller (BET) surface area analysis was employed to reveal the porous structure and the nitrogen adsorption isotherm of the samples with a Micromeritics ASAP 2020 system (Micromeritics Instrument Ltd., Norcross, GA, USA). All the samples were degassed under vacuum at 300 °C for 6 h. The average pore size and the pore volume of the samples were calculated using the Barrett–Joyner–Halenda method. The BET surface area was determined using the BET method.

The morphological features of the sample were analyzed using a Tecnai G2 F20 TEM (FEI, Hillsboro, OR, USA) operating at 200 kV. The distribution of Ni metal and SiO_2 support on the catalyst was examined using high-angle annular dark field scanning TEM (HAADF-STEM) (FEI, Hillsboro, OR, USA). Before performing the TEM measurements, the catalyst powder was dispersed in ethanol using ultrasonic cleaners at room temperature for 30 min.

H_2-TPR experiment was conducted in a quartz tube reactor using 0.1 g of the catalyst samples. Before performing the analysis, all samples were degassed at 110 °C for 4 h. TPR measurements were performed in 10% H_2/Ar mixture, with a gas flow of 40 mL/min, heating rate of 10 °C/min, and reduction temperature ranging from room temperature to 900 °C.

TGA of the samples was performed with a TGA/DTA system (SDT Q600, TA Instruments, new castle, DE, USA) by heating the samples from room temperature to 900 °C in O_2 flow of 10 mL/min.

3.3. Evaluation of the Catalyst Performance

The catalyst activity of Ni@SiO_2 and Ni/SiO_2 for CO methanation was evaluated. Syngas methanation was carried out in a stainless steel tube having an internal diameter of 10 mm in a fixed-bed reactor at 1.5 MPa pressure. The catalytic performance test was performed at the temperature of range of 250 °C–550 °C with an increase of 50 °C in each step.

Initially, a certain amount of Ni@SiO_2 catalyst (0.14 g, 100 mesh) was placed in the upper filling medium quartz sand (30 mesh), in a stainless steel tubular reactor (length: 40 cm, inner diameter: 10 mm). The Ni@SiO_2 catalyst was purged with N_2 30 mL/min. Before performing the test, the catalyst was treated with online reduction, at 500 °C, (reduction of pure hydrogen gas, flow rate of 50 mL/min, for 2 h). After the reduction, when the temperature was decreased to 250 °C, the feed syngas (H_2:N_2:CO molar ratio of 3:1:1) was introduced, In order to analyze the gaseous products obtained; the products were analyzed using gas chromatography techniques.

In order to evaluate the CO conversion and the CH_4 selectivity, at each temperature, the outlet gases were collected and analyzed after 30 min of steady-state operation. The CO conversion (X_{CO}) and CH_4 selectivity (S_{CH_4}) are defined as follows:

$$\text{CO Conversion } (\%) = \frac{n_{CO(in)} - n_{CO(out)}}{n_{CO(in)}} \times 100\% \quad (1)$$

$$\text{CH}_4\text{ Selectivity } (\%) = \frac{n_{CH_4(out)}}{n_{CO(in)} - n_{CO(out)}} \times 100\% \quad (2)$$

$$CH_4\ \text{Yield}\ (\%) = X_{CO} \times S_{CH_4} \times 100\% = \frac{n_{CH_4(out)}}{n_{CO(in)}} \times 100\% \quad (3)$$

4. Conclusions

In summary, core-shell structured Ni@SiO_2 catalysts were prepared using the modified Stöber method. The obtained Ni@SiO_2 catalyst particles exhibited higher catalytic activity than that of the Ni/SiO_2 catalyst prepared by the conventional impregnation method. Under the operation conditions employed (1.5 MPa, $H_2/CO/N_2$ = 3:1:1), nearly 100% CO conversion was achieved over the Ni@SiO_2 catalyst sample along with a CH_4 yield of ~90% (400–500 °C). In the 100-h stability test, the core-shell structure of Ni@SiO_2 shows excellent stability; CO conversion is always greater than 95%. The enhanced performance obtained for Ni@SiO_2 could be mainly attributed to the stronger interaction of the Ni@SiO_2 catalyst. Particles having highly uniform-sized Ni particles Furthermore, TGA results demonstrated that the core-shell structure might cause a reduction in the production of C deposits on the surface of the Ni active component.

Acknowledgments: This research was financially supported by the National Natural Science Funds of China (NSFC, U1203293). The Doctor Foundation of Bingtuan (2013BB010), and the Foundation of Young Scientist in Shihezi University (2013ZRKXJQ03).

Author Contributions: M.Z. designed and administered the experiments; Y.H. performed experiments; B.W. collected data; M.Z. and Y.H. analyzed data and wrote the paper.

Conflicts of Interest: The authors declare no conflict of interest.

References

1. Dai, B.; Wen, B.; Zhu, M.Y.; Kang, L.H.; Yu, F. Nickel catalysts supported on aminofunctionalized MCM-41 for syngas methanation. *RSC Adv.* **2016**, *6*, 66957–66962. [CrossRef]
2. Delgado, K.H.; Maier, L.; Tischer, S.; Zellner, A.; Stotz, H.; Deutschmann, O. Surface reaction kinetics of steam-and CO_2-reforming as well as oxidation of methane over nickel-based catalysts. *Catalysts* **2015**, *5*, 871–904. [CrossRef]
3. Tao, M.; Meng, X.; Lv, Y.H.; Bian, Z.C.; Xin, Z. Effect of impregnation solvent on Ni dispersion and catalytic properties of Ni/SBA-15 for CO methanation reaction. *Fuel* **2016**, *165*, 289–297. [CrossRef]
4. Jin, G.J.; Gu, F.N.; Liu, Q.; Wang, X.Y.; Jia, L.H.; Xu, G.W.; Zhong, Z.Y.; Su, F.B. Highly stable Ni/SiC catalyst modified by Al_2O_3 for CO methanation reaction. *RSC Adv.* **2016**, *6*, 9631–9639. [CrossRef]
5. Zhang, J.Y.; Xin, Z.; Meng, X.; Tao, M. Synthesis, characterization and properties of anti-sintering nickel incorporated MCM-41 methanation catalysts. *Fuel* **2013**, *109*, 693–701. [CrossRef]
6. Bian, L.; Wang, W.H.; Xia, R.; Li, Z.H. Ni-based catalyst derived from Ni/Al hydrotalcitelike compounds by the urea hydrolysis method for CO methanation. *RSC Adv.* **2016**, *6*, 677–686. [CrossRef]
7. Liu, Q.; Zhong, Z.Y.; Gu, F.N.; Wang, X.Y.; Lu, X.P.; Li, H.F.; Xu, G.W.; Su, F.B. CO methanation on ordered mesoporous Ni–Cr–Al catalysts: Effects of the catalyst structure and Cr promoter on the catalytic properties. *J. Catal.* **2016**, *337*, 221–232. [CrossRef]
8. Gao, Y.; Meng, F.H.; Ji, K.M.; Song, Y.; Li, Z. Slurry phase methanation of carbon monoxide over nanosized Ni–Al_2O_3 catalysts prepared by microwave-assisted solution combustion. *Appl. Catal. A* **2016**, *510*, 74–83. [CrossRef]
9. Li, S.; Jin, H.G.; Gao, L.; Zhang, X.S. Exergy analysis and the energy saving mechanism for coal to synthetic/substitute natural gas and power cogeneration system without and with CO_2 capture. *Appl. Energy* **2014**, *130*, 552–561. [CrossRef]
10. Kopyscinski, J.; Schildhauer, T.J.; Biollaz, S.M.A. Production of synthetic natural gas (SNG) from coal and dry biomass—A technology review from 1950 to 2009. *Fuel* **2010**, *89*, 1763–1783. [CrossRef]
11. Li, Y.K.; Zhang, Q.F.; Chai, R.J.; Zhao, G.F.; Cao, F.H.; Liu, Y.; Lu, Y. Metal-foam-structured Ni–Al_2O_3 catalysts: Wet chemical etchingpreparation and syngas methanation performance. *Appl. Catal. A* **2016**, *510*, 216–226. [CrossRef]

12. Lucchini, M.A.; Testino, A.; Kambolis, A.; Proff, C.; Ludwig, C. Sintering and coking resistant core-shell microporous silica-nickel nanoparticles for CO methanation: Towards advanced catalysts production. *Appl. Catal. B* **2016**, *182*, 94–101. [CrossRef]
13. Yan, X.L.; Liu, Y.; Zhao, B.R.; Wang, Z.; Wang, Y.; Liu, C.J. Methanation over Ni/SiO_2: Effect of the catalyst preparation methodologies. *Appl. Catal. B* **2013**, *38*, 2283–2291. [CrossRef]
14. Miyao, T.; Tanaka, J.; Shen, W.; Hayashi, K.; Higashiyama, K.; Watanabe, M. Catalytic activity and durability of a mesoporous silica-coated Ni-alumina-based catalyst for selective CO methanation. *Catal. Today* **2015**, *251*, 81–87. [CrossRef]
15. Wang, C.; Zhai, P.; Zhang, Z.C.; Zhou, Y.; Zhang, J.K.; Zhang, H.; Shi, Z.J.; Han, R.P.S.; Huang, F.Q.; Ma, D. Nickel catalyst stabilization via graphene encapsulation for enhanced methanation reaction. *J. Catal.* **2016**, *334*, 42–51. [CrossRef]
16. Takenaka, S.; Umebayashi, H.; Tanabe, E.; Matsune, H.; Kishida, M. Specific performance of silica-coated Ni catalysts for the partial oxidation of methane to synthesis gas. *J. Catal.* **2007**, *245*, 392–400. [CrossRef]
17. Li, L.; He, S.C.; Song, Y.Y.; Zhao, J.; Ji, W.J.; Au, C.T. Fine-tunable Ni@porous silica core–shell nanocatalysts: Synthesis, characterization, and catalytic properties in partial oxidation of methane to syngas. *J. Catal.* **2012**, *288*, 54–64. [CrossRef]
18. Takenaka, S.; Orita, Y.; Umebayashi, H.; Matsune, H.; Kishida, M. High resistance to carbon deposition of silica-coated Ni catalysts in propane stream reforming. *Appl. Catal. A* **2008**, *351*, 189–194. [CrossRef]
19. Takenaka, S.; Shimizu, T.; Otsuka, K. Complete removal of carbon monoxide in hydrogen-rich gas stream through methanation over supported metal catalysts. *Int. J. Hydrog. Energy* **2004**, *29*, 1065–1073. [CrossRef]
20. Li, S.; Tuel, A.; Laprune, D.; Meunier, F.; Farrusseng, D. Transition-metal nanoparticles in hollow zeolite single crystals as bifunctional and size-selective hydrogenation catalysts. *Chem. Mater.* **2015**, *27*, 276–282. [CrossRef]
21. Park, J.C.; Bang, J.U.; Lee, J.; Ko, C.H.; Song, H. $Ni@SiO_2$ yolk-shell nanoreactor catalysts: High temperature stability and recyclability. *J. Mater. Chem.* **2010**, *20*, 1217–1388.
22. Wang, Z.Y.; Wu, R.F.; Zhao, Y.X. Effect of ZrO_2 promoter on structure and catalytic activity of the Ni/SiO_2 catalyst for CO methanation in hydrogen-rich gases. *Catal. Today* **2010**, *158*, 470–474. [CrossRef]
23. Lakshmanan, P.; Kim, M.S.; Park, E.D. A highly loaded $Ni@SiO_2$ core–shell catalyst for CO methanation. *Appl. Catal. A* **2016**, *513*, 98–105. [CrossRef]
24. Gao, J.J.; Wang, Y.L.; Ping, Y.; Hu, D.C.; Xu, G.W.; Gu, F.N.; Su, F.B. A thermodynamic analysis of methanation reactions of carbon oxides for the production of synthetic natural gas. *RSC Adv.* **2012**, *2*, 2358–2368. [CrossRef]
25. Miyao, T.; Sakurabayashi, S.; Shen, W.; Higashiyama, K.; Watanabe, M. Preparation and catalytic activity of a mesoporous silica-coated Ni-alumina-based catalyst for selective CO methanation. *Catal. Commun.* **2015**, *58*, 93–96. [CrossRef]
26. Shinde, V.M.; Madras, G. CO methanation toward the production of synthetic natural gas over highly active Ni/TiO_2 catalyst. *AIChE J.* **2014**, *60*, 1027–1035. [CrossRef]
27. Zhang, J.Y.; Xin, Z.; Meng, X.; Lv, Y.H.; Tao, M. Effect of MoO_3 on structures and properties of $Ni\text{-}SiO_2$ methanation catalysts prepared by the hydrothermal synthesis method. *Ind. Eng. Chem. Res.* **2013**, *52*, 14533–14544. [CrossRef]
28. Li, L.; Yao, Y.; Sun, B.; Fei, Z.Y.; Xia, H.; Zhao, J.; Ji, W.J.; Au, C.T. Highly active and stable lanthanum-doped core–shell structured $Ni@SiO_2$ catalysts for the partial oxidation of methane to syngas. *ChemCatChem* **2013**, *5*, 3781–3787. [CrossRef]
29. Guan, B.Y.; Wang, X.; Xiao, Y.; Liu, Y.L.; Huo, Q.S. A versatile cooperative template-directed coating method to construct uniform microporous carbon shells for multifunctional core–shell nanocomposites. *Nanoscale* **2013**, *5*, 2469–2475. [CrossRef] [PubMed]
30. Shi, P.; Liu, C.J. Characterization of silica supported nickel catalyst for methanation with improved activity by room temperature plasma treatment. *Catal. Lett.* **2009**, *133*, 112–118. [CrossRef]